Nuclear Inst. and Methods in Physics Research, A 978 (2020) 164401

Contents lists available at ScienceDirect

Nuclear Inst. and Methods in Physics Research, A

journal homepage: www.elsevier.com/locate/nima

Particle tracking and radiation field characterization with Timepix3 in ATLAS

B. Bergmann [a], T. Billoud [a,*], P. Burian [a,b], C. Leroy [c], P. Mánek [a,d], L. Meduna [a,b], S. Pospíšil [a], M. Suk [a]

[a] Institute of Experimental and Applied Physics, Czech Technical University in Prague, Prague 128 00, Czech Republic
[b] Faculty of Electrical Engineering, University of West Bohemia, Univerzitní 8, Pilsen 301 00, Czech Republic
[c] Group of Particle Physics, University of Montreal, Montreal, QC H3T 1J4T, Canada
[d] Department of Physics & Astronomy, University College London, Gower Street, London, WC1E 6BT, United Kingdom

ARTICLE INFO

Keywords:
Radiation monitoring
Solid state detectors
Pixel detectors
dE/dX
Particle tracking

ABSTRACT

Four hybrid pixel detectors of Timepix3 technology, installed in the ATLAS experiment, were continuously taking data from April 2018 until the end of the Run-2 data taking period (December 2019). These detectors are synchronized with each other and the LHC orbit clock. They are capable of resolving the bunch structure of the LHC beams due to their time resolution of ~ 2 ns. Thus, they allow the characterization of the radiation field inside and outside bunch-crossing periods. This is shown for Timepix3 detectors at the extended barrel (x=-3.58 m, y=0.97 m, z=2.83 m). We apply pattern recognition methods to decompose the radiation field and determine the directionality of the minimum ionizing particles (MIP) component of the radiation field.

1. Introduction

The high rate of collisions at the LHC generates an intense radiation field inside the experiments, resulting in various adverse effects such as single event effects, material activation and detector damages. Due to their different designs, each experiment has a unique radiation environment, composed of varying gradients of particle fluxes and complex mixes of particle types and energies. These aspects are commonly predicted using Monte Carlo simulation tools, allowing the design of radiation shielding components and the choice of sufficiently radiation-hard detectors [1]. However, predictions come with some degrees of uncertainty and need to be benchmarked by measurement once the beam is in operation.

In ATLAS, several sets of radiation monitors are dedicated to this task. For example, field-effect transistors are used for dosimetry in the inner tracker, while proportional tubes and scintillators are dedicated to neutron fluence monitoring in the muon spectrometer [2]. In addition to these radiation monitor standards, a detector network based on the Timepix ASIC technology has been operated since 2008, using the advantages of pixelated detectors for characterizing the radiation fields. During Run-2 (2015–2019), the ATLAS-TPX network was used to measure thermal neutron and minimum-ionizing particle (MIP) fluences, as well as the directionality of the MIP field [3]. In parallel to this network, the latest generation of the ASIC family, Timepix3 [4] was tested during 2018 and 2019 in view of an upgrade for ATLAS Run-3. In this paper, we present results from these tests and discuss improvements brought by this new technology. These tests already brought valuable results as reported for instance in [5].

We briefly introduce the Timepix3 technology and describe the algorithms used for data analysis. We then present the capability to measure the radiation components during and in-between the LHC bunch crossings. Finally, we present measurements of MIP directionality and explain how Timepix3 simplifies the methodology compared to the previous detector generation. The measurements presented here were done in nominal LHC conditions with proton–proton collisions at $\sqrt{s} = 13$ TeV.

2. The Timepix3 detectors

Four Timepix3 detectors with 500 μm thick silicon sensors were operated in ATLAS during 2018, each of them being synchronized with the LHC orbit clock, as described in Ref. [6]. Two detectors (I4 and J4) were placed on the external wall of the Tile barrel calorimeter (side A). The other detectors (I3 and H3) were fixed on the outer cavern wall, with the aim to measure the radiation escaping the ATLAS detector. The positions are summarized in Table 1.

Timepix3 [4] is the successor of the Timepix ASIC [7] (which was used in the ATLAS-TPX network since 2015) and presents key advantages for characterizing mixed radiation fields. First, while also featuring a matrix of 256 x 256 pixels with a 55 μm pitch, Timepix3 can measure in data-driven mode. In contrast to the Timepix frame-based

* Corresponding author.
E-mail address: thomas.billoud@utef.cvut.cz (T. Billoud).

https://doi.org/10.1016/j.nima.2020.164401
Received 1 March 2020; Received in revised form 4 May 2020; Accepted 27 May 2020
Available online 18 July 2020

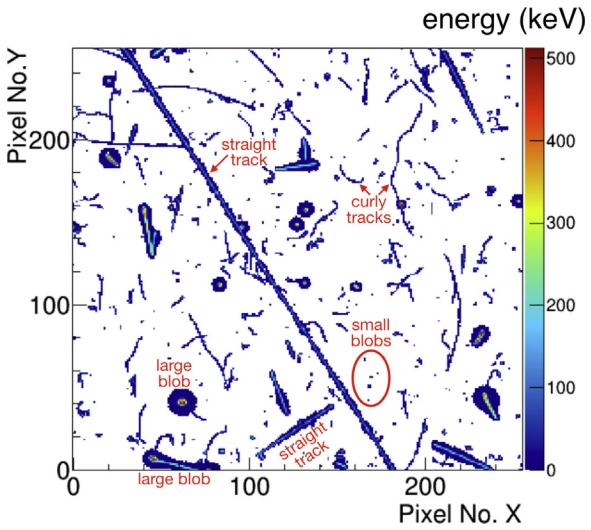

Fig. 1. Snapshot of the radiation field measured by detector J4. Different track shapes are categorized for radiation field characterization. Example events are labeled.

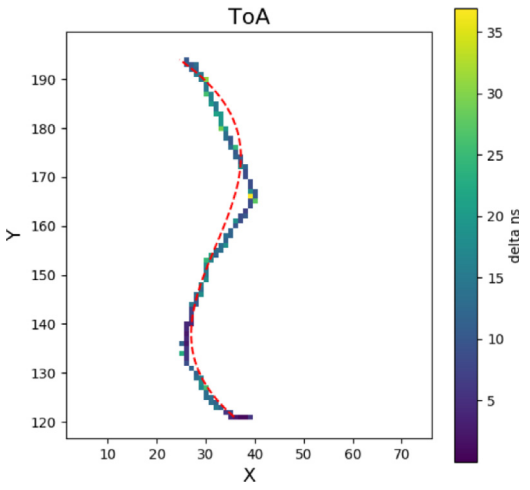

Fig. 2. Illustration of polynomial interpolation used for distinguishing curly tracks from straight tracks. The red-dashed line corresponds to the fitted polynomial. The original event is displayed with time-of-arrival (ToA) in nanoseconds on the *z*-axis, *delta* being the ToA with respect to the lowest ToA in the cluster.

Table 1
Overview of the Timepix3 positions in ATLAS. The data of devices J4 and I4 are presented and discussed in the text. The corresponding results of the other two detectors are shown in Appendix.

Chip ID	X [mm]	Y [mm]	Z [mm]
J4	−3580	970	2830
I4	−3580	970	2830
I3	4000	3400	22,900
H3	4000	3400	22,900

readout, this mode allows deadtime-free operation, given that interactions do not overlap during the pixel readout time (∼500 ns). Another advantage is that each pixel can simultaneously measure the deposited energy as well as time-of-arrival, which improves the reconstruction efficiency of analysis algorithms. Finally, the time-stamping precision of Timepix3 (1.6 ns) allows the distinction between radiation field particles generated during LHC bunch crossings, and those produced in between by secondary interactions.

The Timepix3 detectors were calibrated on a per-pixel basis using mono-energetic X-ray sources, with energies ranging from 3 keV to 60 keV. The time-of-arrival measurements were corrected for time-walk effects using 60 keV X-rays [8]. The data sets were recorded in 3 h time intervals and were subjected to a noisy pixel removal procedure: each pixel counting more than 3 σ from the mean pixel count was excluded from analysis [5].

3. Analysis methods

While the methods used for the presented analysis resemble those of the ATLAS-TPX network [3], they include newly developed algorithms adapted for the data-driven mode of Timepix3. The dedicated cluster finding methodology is described in [9]. It searches for coincident pixels in time and space. The clusters are further divided into four classes according to their morphology, as illustrated in Fig. 1. Small blobs consist of few adjacent pixels and correspond to relativistic low-Z particles (MIPs) hitting the sensor surface perpendicularly, X-rays or low energy electrons. γ-rays and energetic electrons typically leave curly tracks, which are differentiated from straight tracks using a polynomial interpolation. This interpolation provides a sufficient metric for cluster curvature and linearity, as illustrated in Fig. 2.

Straight tracks, in turn, correspond to MIPs going through the sensor entirely. Their impact point is determined by comparing the carrier drift times at the track end points. The impact angle is calculated from the track length. Finally, large blobs are the trace of particles with high energy deposition in the sensor (high energy transfer events, HETE), for example low energy protons or the products of nuclear interactions inside or around the detector.

4. Bunch crossing identification

The 1.6 ns time granularity of Timepix3 and its synchronization with the LHC orbit clock allows, up to a certain extent, to distinguish radiation emitted during bunch crossings from radiation resulting from secondary effects. The latter are a mixture of particles produced by beam–gas interactions [10], by the crossing of satellite and ghost bunches [11], and by material activation. Fig. 3(a) shows the measured cluster rate as a function of time in the LHC orbit as seen in the inner detectors I4 and J4. Due to the small solid angle covered by the outer detectors (I3 and H3) and the higher ratio of background events, the bunch structure cannot be resolved properly with H3 and I3. The LHC revolution frequency being 11.2 kHz, the bunch crossing scheme repeats every 89 μs. Bunches are grouped in so-called trains in which they are separated by 25 ns, as revealed in Fig. 3(a).

It can be seen that bunch crossings lead to a ∼30% increase of the measured cluster rate. The peaks sit on a background of particles from activation of the surrounding material or from non-relativistic particles (e.g. moderated neutrons). The peak is widened by the time resolution of the detector, which depends on the particle type.[1] For MIPs, the time resolution is ∼2 ns [12]. For photons, neutrons, and particles stopped inside the sensor volume, drift time fluctuations up to ∼25 ns can smear out the peak structure.

Fig. 3(b) shows a detailed view of a single bunch crossing with characteristic tracks selected inside and outside the peak area. Apart from the difference in cluster quantities, no clear distinction between cluster morphologies can be visually made. For a quantitative comparison of the radiation components, one can compare the cluster types between these two regions. This is shown in Fig. 4, with the populations of clusters during bunch crossings (*peak region*) and background clusters. The cluster populations are dominated by small blobs and curly tracks, which correspond to X-rays, γ-rays and electrons. The largest difference between the peak and background regions occurs for straight tracks, which correspond to MIPs, i.e. mainly protons, electrons, pions and muons. Hence, these are a clean trace of proton–proton interactions.

[1] because of drift time variations depending on interaction depth in the 500 μm thick silicon sensors.

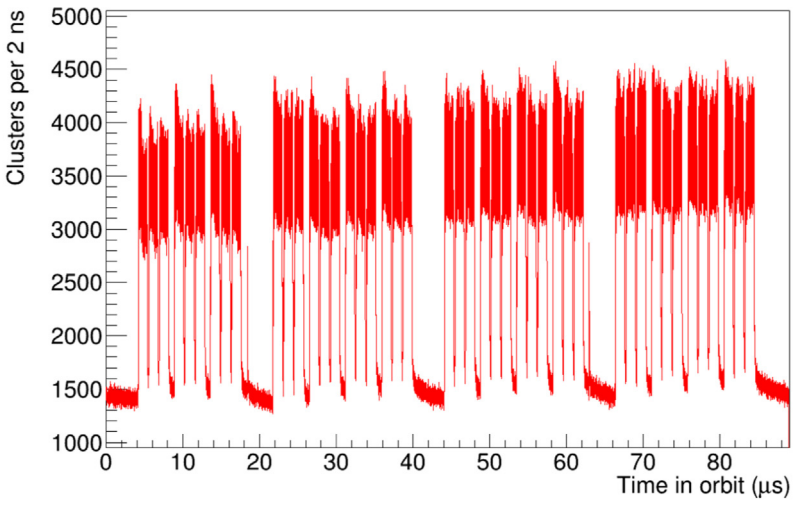

(a)

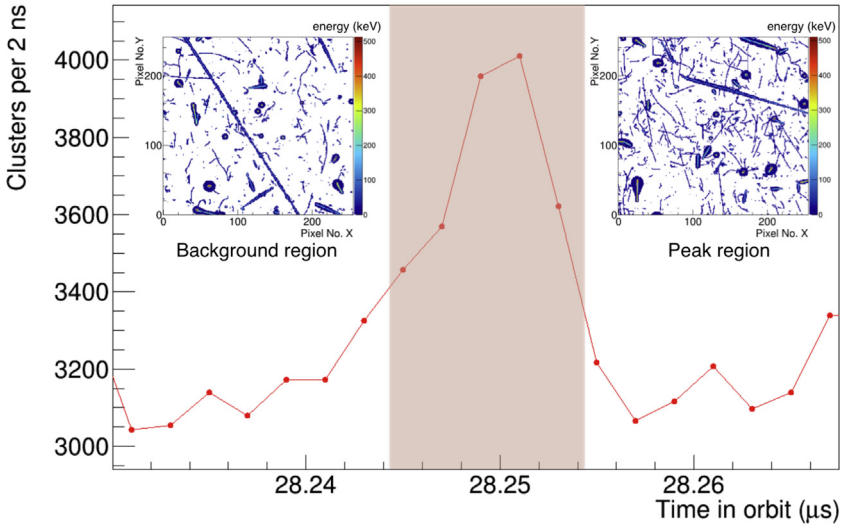

(b)

Fig. 3. (a) Number of clusters as a function of the reference time in the LHC beam orbit. The LHC frequency being 11.2 kHz, the reference time goes from 0 to 89 μs, with a bunch spacing of 25 ns (inside the so-called bunch trains); On the *y*-axis, the cluster counts are integrated over an entire run (integrated luminosity: 393 pb^{-1}). (b) Zoom to a single bunch. The pixel matrices show snapshots of the radiation field in the peak region (*red shaded*) and the background region. The data was measured with I4 and J4 during ATLAS Fill 6696 (Run: 350479) on May 17, 2018. (For interpretation of the references to color in this figure legend, the reader is referred to the web version of this article.)

5. MIP tracking

In this section, we present the measurement capabilities for MIP-like particles. Clusters corresponding to these particles are distinguishable by their linearity, using the fitting algorithm described in Section 3. Incomplete tracks at the edges of the sensor and tracks with a *roundness*[2] bigger than 0.5 were omitted.

5.1. Measured dE/dX spectra

Fig. 5 gives the stopping power (dE/dX) distribution of particles with high linearity in the 500 μm thick silicon sensor layer. The stopping power is calculated as:

$$\frac{dE}{dX} = \frac{E_{\text{dep}}}{\rho_{\text{Si}} \times L}, \tag{1}$$

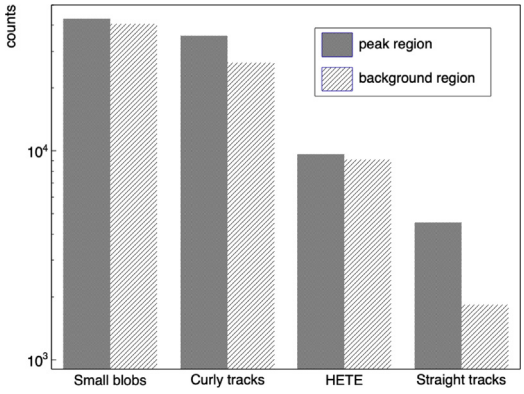

Fig. 4. Comparison of cluster types during and in-between bunch-crossings. The time windows where cluster are selected are set to 10 ns both for the peak region and background region (see Fig. 3).

[2] Roundness is defined as $roundness = size/(\pi r^2)$, where $roundness \in [0, 1]$ (1 means perfectly round cluster). $Size$ is the number of pixels in the cluster and $2r$ is euclidian pixel distance of the two most distant pixels in the cluster.

where E_{dep} is the energy deposition of the track and $\rho_{\text{si}} = 2.33\ \frac{\text{g}}{\text{cm}^3}$ the density of the silicon sensor. The track length is given as $L =$

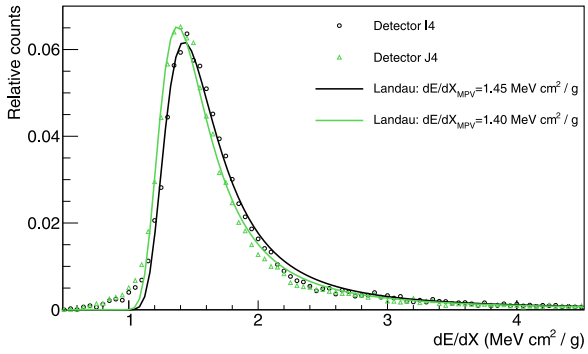

Fig. 5. Stopping power of particles identified as MIPs (200 000 samples used). The distributions are modeled with the Landau implementation of ROOT [13] with most probable values of 1.45 MeV (detector I4) and 1.40 MeV (detector J4).

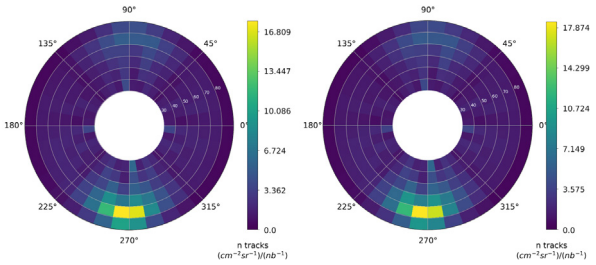

Fig. 6. Incident angles of MIPs measured by the four Timepix3 detectors installed in ATLAS. θ and ϕ represent the polar and azimuthal angles between the interaction point and the sensor surface, respectively. The z-axis is the number of MIPs normalized to effective area, solid angle and integrated luminosity.

$\sqrt{\Delta x^2 + \Delta y^2 + t^2}$, where Δx and Δy are the extensions of the track in the 2D projection plane and $t = 500$ µm is the sensor thickness. The spectra follow Landau–Vavilov distributions with a most probable value of $\sim 1.4 \frac{\text{MeV cm}^2}{\text{g}}$, which is characteristic for MIPs in silicon.

5.2. MIP directions

An aspect of the radiation field that can be studied exclusively with pixelated detectors is the directionality of the MIP field. A similar study has already been done for the Timepix network (ATLAS-TPX) [3,14]. While 2 layers were needed to resolve the ambiguity of the θ angle, the additional drift time information available with Timepix3 allows the use of a single layer.[3]

The incident directions of MIPs are displayed in Fig. 6, where the polar (θ) and azimuthal (ϕ) angles are represented by polar axes. The z-axis gives the particle count, which is normalized to three parameters:

1. the effective area, dividing each particle weight by $\cos(\theta)$.
2. the solid angle, calculated for each histogram bin.
3. the integrated luminosity, obtained from the LUCID detector [15].

The excess of events on the bottom of the figures correspond to MIPs coming from the interaction point and from secondary interactions in the vicinity of this axis of incidence. The latter might be, for example, energetic protons or pions generated during particle showers in the calorimeters, in-between the interaction point and the Timepix3 detectors. A slight excess is also observed with opposite azimuthal angle ($\theta \approx 70°, \phi \approx 90°$). These events are likely due to MIPs originating from the LAr forward calorimeter, which is known to be a major source of radiation [1].

Because MIPs hitting the Timepix3 sensors perpendicularly leave clusters that are similar to those corresponding to X-rays and low energy electrons (i.e. short straight tracks), they are rejected by the pattern recognition algorithms. This sets a lower polar angle (θ) limit at 30°, as indicated with the whitened center in (a) and (b) of Fig. 6. For ATLAS Run-3, this limitation will be overcome by using coincidence information of two stacked sensors, as was done with the previous Timepix detector generation.

[3] The traveling direction, i.e. whether the MIP arrives from the front-side or back-side of the detector, is still undetermined.

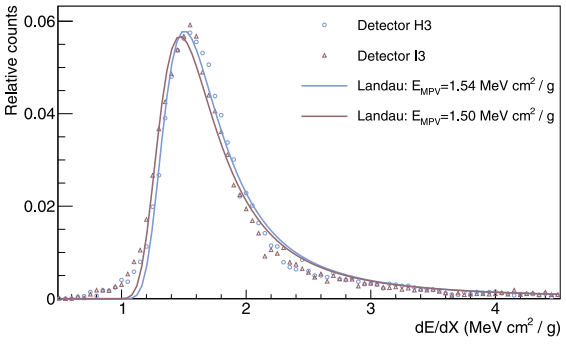

Fig. A.7. Same as Fig. 5, but for detectors H3 and I3.

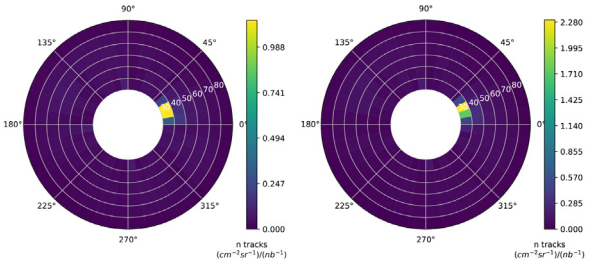

Fig. A.8. Same as Fig. 6 but for detectors H3 and I3.

6. Summary and outlook

Timepix3 detectors allow one to characterize the radiation field in ATLAS on the time scale of individual LHC bunch crossings. In particular, it is possible to track MIPs and reconstruct their incident angles, which gives a clean signal of proton collisions at the interaction point. This could be particularly valuable for luminosity measurements [5], where the need for beam background suppression is of primary importance.

In view of the upcoming ATLAS Run-3, it is proposed to install telescopes of Timepix3 detectors, with sensors facing each other as close as possible. This will allow a full solid angle coverage for MIP detection and improve the radiation recognition potential, leading to more precise benchmarking of radiation field simulations.

Declaration of competing interest

The authors declare that they have no known competing financial interests or personal relationships that could have appeared to influence the work reported in this paper.

Acknowledgments

The work was done within the Medipix collaboration. It was supported by the European Regional Development Fund-Projects "Van de Graaff Accelerator - a Tunable Source of Monoenergetic Neutrons and Light Ions" (No. CZ.02.1.01/0.0/0.0/16_013/0001785), "Engineering applications of physics of microworld" (No. CZ.02.1.01/0.0/0.0/16_019/0000766), and the Ministry of Education, Youth and Sports of the Czech Republic under "RICE - New Technologies and Concepts for Smart Industrial Systems", project No. LO1607. The support of NSERC-Canada is also acknowledged.

Appendix. Stopping power and angle maps for H3 and I3

See Figs. A.7 and A.8.

References

[1] S. Baranov, M. Bosman, I. Dawson, V. Hedberg, A. Nisati, M. Shupe, Estimation of Radiation Background, Impact on Detectors, Activation and Shielding Optimization in ATLAS, Tech. Rep. ATL-GEN-2005-001, ATL-COM-GEN-2005-001, CERN-ATL-GEN-2005-001, CERN, Geneva, Switzerland, 2005.

[2] The ATLAS Collaboration, The ATLAS experiment at the CERN Large Hadron Collider, J. Instrum. 3 (08) (2008) S08003, http://dx.doi.org/10.1088/1748-0221/3/08/s08003.

[3] B. Bergmann, T. Billoud, C. Leroy, S. Pospisil, Characterization of the radiation field in the ATLAS experiment with timepix detectors, IEEE Trans. Nucl. Sci. 66 (7) (2019) 1861–1869, http://dx.doi.org/10.1109/TNS.2019.2918365.

[4] T. Poikela, J. Plosila, T. Westerlund, M. Campbell, M.D. Gaspari, X. Llopart, V. Gromov, R. Kluit, M. van Beuzekom, F. Zappon, V. Zivkovic, C. Brezina, K. Desch, Y. Fu, A. Kruth, Timepix3: a 65k channel hybrid pixel readout chip with simultaneous toa/tot and sparse readout, J. Instrum. 9 (05) (2014) C05013, http://dx.doi.org/10.1088/1748-0221/9/05/C05013.

[5] B. Bergmann, T. Billoud, P. Burian, P. Broulim, C. Leroy, C. Lesmes, P. Manek, L. Meduna, S. Pospisil, A. Sopczak, M. Suk, Relative luminosity measurement with timepix3 in ATLAS, J. Instrum. 15 (01) (2020) C01039, http://dx.doi.org/10.1088/1748-0221/15/01/C01039.

[6] P. Burian, P. Broulím, B. Bergmann, V. Georgiev, S. Pospíšil, L. Pušman, J. Zich, Timepix3 detector network at ATLAS experiment, J. Instrum. 13 (11) (2018) C11024, http://dx.doi.org/10.1088/1748-0221/13/11/c11024.

[7] X. Llopart, R. Ballabriga, M. Campbell, L. Tlustos, W. Wong, Timepix, a 65k programmable pixel readout chip for arrival time, energy and/or photon counting measurements, Nucl. Instrum. Methods Phys. Res. A 581 (1–2) (2007) 485–494, http://dx.doi.org/10.1016/j.nima.2007.08.079.

[8] B. Bergmann, M. Pichotka, S. Pospisil, J. Vycpalek, P. Burian, P. Broulim, J. Jakubek, 3d track reconstruction capability of a silicon hybrid active pixel detector, The Eur. Phys. J. C 77 (6) (2017) 421, http://dx.doi.org/10.1140/epjc/s10052-017-4993-4.

[9] L. Meduna, B. Bergmann, P. Burian, P. Mánek, S. Pospíšil, M. Suk, Real-time timepix3 data clustering, visualization and classification with a new clusterer framework, 2019, arXiv:1910.13356.

[10] A. Alexopoulos, C. Barchel, A. Bay, F. Blanc, E. Bravin, G. Bregliozzi, N. Chritin, B. Dehning, M. Ferro-Luzzi, S. Gianì, M. Giovannozzi, O. Girard, R. Greim, G. Haefeli, P. Hopchev, R. Jacobsson, L. Jensen, O. Rhodri Jones, V.e.a. Kain, First LHC transverse beam size measurements with the beam gas vertex detector, J. Phys.: Conf. Ser. 874 (CERN-ACC-2017-315. 1) (2017) http://dx.doi.org/10.1088/1742-6596/874/1/012086, 012086. 6p. URL http://cds.cern.ch/record/2276055.

[11] A. Jeff, M. Andersen, A. Boccardi, S. Bozyigit, E. Bravin, T. Lefevre, A. Rabiller, F. Roncarolo, C.P. Welsch, A.S. Fisher, Measurement of satellite bunches at the LHC, Conf. Proc. C1205201 (CERN-ATS-2012-088) (2012) MOEPPB010. 3p. URL https://cds.cern.ch/record/1459107.

[12] P. Burian, P. Broulím, V. Georgiev, B. Bergmann, S. Pospíšil, Particle telescope with timepix3 pixel detectors, J. Instrum. 13 (01) (2018) C01002, http://dx.doi.org/10.1088/1748-0221/13/01/c01002.

[13] R. Brun, F. Rademakers, ROOT — AN object oriented data analysis framework, Nucl. Instrum. Methods Phys. Res. A 389 (1) (1997) 81–86, http://dx.doi.org/10.1016/S0168-9002(97)00048-X.

[14] P. Mánek, B.L. Bergmann, P. Burian, L. Meduna, S. Pospíšil, M. Suk, Randomized computer vision approaches for pattern recognition in timepix and timepix3 detectors, in: 2019 Connecting the Dots and Workshop on Intelligent Trackers, 2019, arXiv:1911.02367.

[15] ATLAS collaboration, Luminosity determination in pp collisions at $\sqrt{s} = 13$ tev using the ATLAS detector at the LHC, 2019.